Chinese Journal of Mechanical Engineering

ORIGINAL ARTICLE

Influence of Shear Effects on the Characteristics of Axisymmetric Wave Propagation in a Buried Fluid-Filled Pipe

Ping Lu[1*] , Xiaozhen Sheng[2], Yan Gao[3] and Ruichen Wang[4]

Abstract

The acoustic propagation characteristics of axisymmetric waves have been widely used in leak detection of fluid-filled pipes. The related acoustic methods and equipment are gradually coming to the market, but their theoretical research obviously lags behind the field practice, which seriously restricts the breakthrough and innovation of this technology. Based on the fully three-dimensional effect of the surrounding medium, a coupled motion equation of axisymmetric wave of buried liquid-filled pipes is derived in detail, a contact coefficient is used to express the coupling strength between surrounding medium and pipe, then, a general equation of motion was derived which contain the pipe soil lubrication contact, pipe soil compact contact and pipe in water and air. Finally, the corresponding numerical calculation model is established and solved used numerical method. The shear effects of the surrounding medium and the shear effects at the interface between surrounding medium and pipe are discussed in detail. The output indicates that the surrounding medium is to add mass to the pipe wall, but the shear effect is to add stiffness. With the consideration of the contact strength between the pipe and the medium, the additional mass and the pipe wall will resonate at a specific frequency, resulting in a significant increase in the radiation wave to the surrounding medium. The research contents have great guiding effect on the theory of acoustic wave propagation and the engineering application of leak detection technology in the buried pipe.

Keywords: Buried fluid-filled pipe, Axisymmetric waves, Shear effect, Dispersion

1 Introduction

With the development of urbanisation in past decades, the component like pipe has become a necessary means of liquid and gas transportation. The issue of plumbing leakage is a widespread concern in both industry and academy due to its social, environmental and economic utility. It has been estimated that, in mainland China, current direct economic losses caused by underground pipe network leaks exceed 200 billion Yuan (approximately 22.65 billion pound sterling), sometimes the pipe leakage might cause unexpected major source of hidden danger not only for damaging urban biological environment and the security of people's lives and properties. The latest research of the 'track and trace' technology for buried pipelines, which is widely used in the transportation of liquid and gas media such as crude oil and natural gas, is being widely discussed and studied extensively. Acoustic detection methods has attracted more attention because of such non-destructive evaluation does not directly destroy the structure of the original piping system [1–8]. When the leaking of the pipeline happened, the high-pressure fluid in the pipe will be pressured out of the pipeline and cause unavoidable noise, The acoustic leak detection method is used to detect the events of leaks in different locations of the pipeline, using cross-correlation technique to estimate the delay of leakage noise between two measuring points, then the location

*Correspondence: 277717386@qq.com
[1] State Key Laboratory of Traction Power, Southwest Jiaotong University, Chengdu 610031, China
Full list of author information is available at the end of the article

Lu *et al. Chinese Journal of Mechanical Engineering*   (2022) 35:74

Page 2 of 10

of leakage would be calculated [9]. The effectiveness of these methods much depends on the rationality of the selection of the propagation characteristic parameters of the dominant wave in the pipeline.

The studies of the acoustic characteristics and propagation mechanism of pipes is developed with pipe leak detection. At present, the acoustic leak detection and location of pipelines are usually carried out by time delay estimation method, which depends strongly on wave propagation characteristics. The early research was mainly to solve the wave equation in thin-walled shell pipe, in which the external medium outside pipes is considered vacuum. Fuller, et al. [10] derived the propagation characteristics of $n = 0$ wave within elastic fluid-filled pipes in vacuo defined as "hard" and "soft" shells, then the energy distribution of radial input force and internal pressure fluctuation under various waveforms is studied theoretically [11]. Xu et al. [12] studied the vibration propagation characteristics of liquid filling pipes in a vacuum environment. Pinnington et al. [13] established an acoustic propagation model of cast iron pipes without considering the dispersion characteristics, after that, studied the $n = 0$ wave propagation characteristic and transfer equation of the pressurised pipes [14, 15]. With the development of pipe research, the influence of the medium around the pipes has gradually attracted people's attention. Sinha et al. [16] studied the numerical results of acoustic wave propagation characteristics of fluid-filled pipes in infinite fluid. Greenspon [17] presented the axisymmetric vibration of thick-wall and thin-walled liquid-filled pipes in water medium. Long et al. [18] put forward a model of acoustic velocity dispersion in the process of acoustic vibration signal propagation and verified by experiments. Zhang, et al. [19] proposed a calculation model for sound velocity under different pipeline embedding conditions. Muggleton et al. [20–22] analysed the propagation characteristics of fluid-dominated axisymmetric waves ($s = 1$, $n = 0$) in filled buried pipes. Gao et al. [23, 24] developed a general expression for the fluid-dominated wavenumber in a thin-walled fluid-filled pipe surrounded by a layered elastic soil, and the influence of load effect on elastic medium around pipeline is considered. Kalkowski et al. [25] present a multi-wave model for propagation in axisymmetric fluid-filled waveguides based on the semi-analytical finite elements. Yan et al. [26] developed an experimental investigation for mapping and locating pipe leakage employing the image fusion of ground surface vibration.

Current research studies reveal that at low frequencies, the fluid-dominated axisymmetric wave is not only the main carrying waveform of the vibration energy within the buried fluid-filled pipe, but also is an effective signal component which can be used for pipe leakage inspection. This waveform corresponds to the breathing mode of the pipeline, and the current researches on the problem are mainly focused on the metal pipeline. Due to the flexibility of the plastic pipe, the coupling between the pipe and the surrounding medium (mainly soil) is significant, making the influence of the acoustic wave propagation speed and the damping characteristics of the surrounding medium on the energy attenuation more complicated. However, such coupling effect has not been properly addressed in the past; especially the actual contact strength of the pipe-medium interface cannot be considered. With the large-scale use of plastic pipes and the frequent leakage hazards in China's urbanisation construction, it is urgent to carry out related research to avoid unnecessary costs.

In this paper, the coupling vibration equation of "soil-pipe-fluid" is derived in detail, the acoustic wave propagation characteristic model of the buried pipeline is established, and the shear effect of the medium outside the pipe and the shear effect of the interface between the pipe and the medium on the axisymmetric wave of the fluid dominant are discussed.

2 Differential Equations of Motion of the Medium-Pipe-Fluid System

2.1 Free Motion Equation of Fluid-Filled Pipe
In this section, the coupled motion equations of fluid dominant axisymmetric waves in a buried fluid-filled pipes are deduced based on the motion equations of the fluid-filled pipe in vacuum [10]. The soil medium around the pipes is regarded as a homogeneous and isotropic elastic medium which allows both compression wave and shear wave to propagate. According to the current research, the $s = 1$ wave is usually the main carrier of energy in the leakage signal therefore of most interest, and the dynamic damping effect of the pipeline is neglected. Figure 1 shows the cylindrical coordinates of pipes, where u, v, w are the shell displacements in the axial (x), circumferential (θ), and radial (r) directions, respectively. a and h are the pipe radius and the wall thickness respectively and is assumed. The internal fluid is assumed to be inviscid, and both the surrounding medium and internal fluid are assumed to be lossless.

For axisymmetric waves ($n = 0$), the rotational motion of the pipe can be neglected, so the circumferential displacement and shear stress are both set to zero, free-motion equation of fluid-filled pipe can be described simply according to Donnell-Mushtari shell equation [27] as follows:

$$\begin{bmatrix} A_{11} & A_{13} \\ A_{31} & A_{33} \end{bmatrix} \begin{pmatrix} u \\ w \end{pmatrix} = \frac{1 - v_p^2}{Eh} \begin{pmatrix} 0 \\ p_f(a) \end{pmatrix}, \tag{1}$$

Lu *et al. Chinese Journal of Mechanical Engineering*　　(2022) 35:74
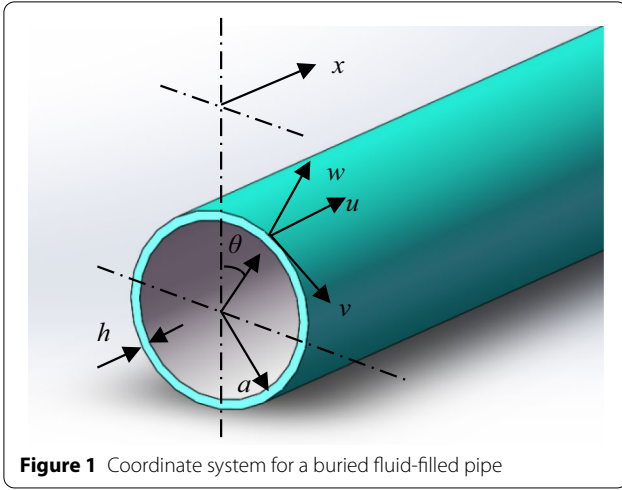
Page 3 of 10

Figure 1 Coordinate system for a buried fluid-filled pipe

where $A_{11} = \frac{\partial^2}{\partial x^2} - \frac{\rho_p(1-\nu_p^2)}{E_p}\frac{\partial^2}{\partial t^2}$; $A_{13} = \frac{\nu_p}{a}\frac{\partial}{\partial x}$; $A_{13} = A_{31}$;

$A_{33} = \frac{1}{a^2} + \delta^2 a^2 \frac{\partial^4}{\partial x^4} + \frac{\rho_p(1-\nu_p^2)}{E_p}\frac{\partial^2}{\partial t^2}$. Here, ρ_p, E_p, ν_p are the density, Young's modulus and Poisson's ratio of the pipe; δ is the stiffness factor, $\delta^2 = h^2/12a^2$; $p_f(a)$ is the internal pressure at fluid pipe interface.

2.2 Motion Equation of Soil Medium

The displacement of soil medium in all directions can be present as $\boldsymbol{u}(x, r, \theta, t)$. For axisymmetric motion, the torsional displacement can be ignored, then $u_\theta = 0$. Travelling wave solutions for the surrounding medium may be assumed of the form:

$$\begin{cases} u_x = U_m \exp(i(\omega t - k_{ns}x)), \\ u_r = W_m \exp(i(\omega t - k_{ns}x)), \end{cases} \quad (2)$$

where W_m, U_m are the amplitude in radial and axial motion of soil medium, which are the functions of radius r.

In the column coordinate system, the expansion process of soil medium can be expressed as

$$\Delta = \frac{1}{r}\frac{\partial}{\partial r}(ru_r) + \frac{\partial u_x}{\partial x}, \quad (3)$$

where $\partial/\partial_\theta = 0$. So, the rotating components of soil medium in the axial and radial direction can also be ignored. The rotating component in the direction θ is

$$\varpi_\theta = \frac{1}{2}\left(\frac{\partial u_r}{\partial x} - \frac{\partial u_x}{\partial r}\right). \quad (4)$$

Substituting for u_r and u_x from Eq. (2) into Eqs. (3) and (4) gives

$$\begin{cases} \Delta = (\frac{\partial W_m}{\partial r} + \frac{W_m}{r} - ik_s U_m)\exp(i(\omega t - k_s x)), \\ \varpi_\theta = \frac{1}{2}(-ik_s W_m - \frac{\partial U_m}{\partial r})\exp(i(wt - k_s x)). \end{cases} \quad (5)$$

According to stresses waves in solids [28], the displacement of a point in the soil medium satisfies the equation of motion

$$(\lambda_m + \mu_m)\nabla(\Delta) + \mu_m \nabla^2 \boldsymbol{u} = \rho_m \frac{\partial^2 \boldsymbol{u}}{\partial \boldsymbol{t}^2}, \quad (6)$$

where λ_m, μ_m are lame coefficients; ρ_m is the density of the medium; ∇ is the Hamilton differential operator.

The motion equation of soil medium can be obtained by combining Eqs. (2)–(6)

$$\begin{cases} \frac{\partial^2 \Delta}{\partial r^2} + \frac{1}{r}\frac{\partial \Delta}{\partial r} + (k_{ds}^r)^2 \Delta = 0, \\ \frac{\partial^2 \varpi_\theta}{\partial r^2} + \frac{1}{r}\frac{\partial \varpi_\theta}{\partial_r} - \frac{\varpi_\theta}{r^2} + (k_{rs}^r)^2 \varpi_\theta = 0, \end{cases} \quad (7)$$

where k_{ds}^r, k_{rs}^r are the compression and shear wavenumbers of soil in radial direction respectively, which can be expressed by compressed wavenumber k_d, shear wavenumber k_r and wavenumber in axil direction k_s as follows:

$$(k_{ds}^r)^2 = k_d^2 - k_s^2, \ (k_{rs}^r)^2 = k_r^2 - k_s^2, \quad (8)$$

where

$$k_d^2 = \rho_m \omega^2/(\lambda_m + 2\mu_m), \ k_r^2 = \rho_m \omega^2/\mu_m.$$

Equation of motion shown in Eq. (7) can be expressed as the Bessel equation of cylindrical space outside the pipe

$$\begin{cases} \Delta = GH_0(k_{ds}^r r), \\ \varpi_\theta = HH_1(k_{rs}^r r), \end{cases} \quad (9)$$

where G, H are the functions of coordinate in the axial (x) and time (t). $H_0(\cdot)$, $H_1(\cdot)$ are the Hankel functions of the second kind which describe outgoing waves.

In order to satisfy Eqs. (5) and (9), U_m, W_m must have the form [24]

$$\begin{cases} U_m = -iA_m k_s H_0(k_{ds}^r r) + iB_m \frac{1}{r}\frac{\partial}{\partial r}[rH_1(k_{rs}^r r)], \\ W_m = A_m \frac{\partial}{\partial r}[H_0(k_{ds}^r r)] - B_m k_s H_1(k_{rs}^r r), \end{cases} \quad (10)$$

where A_m, B_m are constants. Substituting Eq. (2) into Eq. (10) gives

$$\begin{pmatrix} u_x \\ u_r \end{pmatrix} = \boldsymbol{T_1}\begin{pmatrix} A_m \\ B_m \end{pmatrix}\exp(i(\omega t - \boldsymbol{k_s x})), \quad (11)$$

where $\boldsymbol{T_1} = \begin{bmatrix} -ik_s H_0(k_{ds}^r r) & i(k_{rs}^r)^2 H_0(k_{rs}^r r) \\ k_{ds}^r H_0'(k_{ds}^r r) & k_s H_0'(k_{rs}^r r) \end{bmatrix}$, $H_0'(\chi) = \frac{\partial}{\partial \chi}H_0(\chi)$.

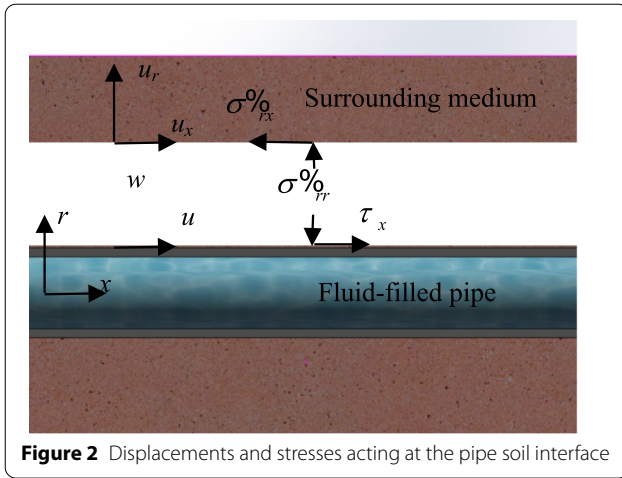According to Hook's law, the relationship between stress and strain in the surrounding medium is

Lu *et al. Chinese Journal of Mechanical Engineering*   (2022) 35:74

Page 4 of 10

Figure 2 Displacements and stresses acting at the pipe soil interface

$$\begin{cases} \tilde{\sigma}_{rx} = \mu_m \left(\frac{\partial u_r}{\partial x} + \frac{\partial u_x}{\partial r} \right), \\ \tilde{\sigma}_{rr} = \lambda_m \Delta + 2\mu_m \frac{\partial u_r}{\partial r}. \end{cases} \quad (12)$$

Substituting Eq. (11) into Eq. (12) gives

$$\begin{pmatrix} \tilde{\sigma}_{rx} \\ \tilde{\sigma}_{rr} \end{pmatrix} = \mathbf{T_2} \begin{pmatrix} A_m \\ B_m \end{pmatrix} \exp(i(\omega t - k_s x)), \quad (13)$$

where $\mathbf{T_2} = \begin{bmatrix} -2i\mu_m k_s k_{ds}^r H_0'(k_{ds}^r r) & i\mu_m(2k_s^2 - k_r^2)H_1(k_{rs}^r r) \\ 2\mu_m(k_{ds}^r)^2 H_0''(k_{ds}^r r) - \lambda_m k_d^2 H_0(k_{ds}^r r) & -2\mu_m k_s k_{rs}^r H_1(k_{rs}^r r) \end{bmatrix}$,
$H_0''(\chi) = \frac{\partial^2}{\partial \chi^2} H_0(\chi)$. Combining Eqs. (10) and (12) and eliminating the potential coefficients A_m, B_m, the relationship between stress and displacement can be expressed by

$$\begin{pmatrix} \tilde{\sigma}_{rx} \\ \tilde{\sigma}_{rr} \end{pmatrix} = \mathbf{T} \begin{pmatrix} u_x \\ u_r \end{pmatrix}. \quad (14)$$

where $\mathbf{T} = \mathbf{T_2} \mathbf{T_1}^{-1}$.

2.3 Coupling Motion Equations of Pipe-Medium

When single axisymmetric waves are considered, the load distribution at the pipe-medium interface is shown in Figure 2. It assumes that the pipe and medium are in constant contact during the course of movement, the radial displacement of the surrounding medium at the pipe interface is assumed the same as that of the pipe-wall, $u_r = w$. The contact stress of pipe and medium in the radial direction are considered as identical, which expressed as $\tilde{\sigma}_{rr}$. The frictional stress along the pipe surface equals the shear stress in the axial direction, which expressed as τ_x. The coupled motion equations given by Eq. (1) can be written as

$$\begin{bmatrix} A_{11} & A_{13} \\ A_{31} & A_{33} \end{bmatrix} \begin{pmatrix} u \\ w \end{pmatrix} = \frac{1 - v_p^2}{Eh} \begin{pmatrix} -\tau_x \\ p_f(a) + \tilde{\sigma}_{rr}(a) \end{pmatrix}. \quad (15)$$

According to Donnell-Mushtari shell equation [29], the displacement of pipe can be expressed

$$\begin{cases} u = U_s \exp(i(\omega t - k_{ns} x)), \\ w = W_s \exp(i(\omega t - k_{ns} x)). \end{cases} \quad (16)$$

Substituting Eq. (16) into Eq. (15) gives

$$\begin{bmatrix} \Omega^2 - (k_s a)^2 & -iv_p(k_s a) \\ -iv_p(k_s a) & 1 - \Omega^2 + \delta^2(k_s a)^4 \end{bmatrix} \begin{pmatrix} u \\ w \end{pmatrix}$$
$$= \frac{1 - v_p^2}{E_p h} a^2 \begin{pmatrix} -\tau_x \\ p_f(a) + \tilde{\sigma}_{rr}(a) \end{pmatrix}, \quad (17)$$

where Ω is the non-dimensional frequency, $\Omega = \omega a/c_L = k_L a$; c_L is the shell compressional wave speed; k_L is the shell compressional wavenumber, $k_L^2 = \omega^2 \rho_p (1 - v_p^2)/E_p$. For a thin-walled pipe $h/a \ll 1$, so $\delta^2(k_s a)^4$ is very small to be ignored. Then, the displacement of the shell can be solved by the pressure in the pipe $p_f(a)$, the shear force between the pipe and the soil τ_x and the compressive stress between the pipe and the soil $\tilde{\sigma}_{rr}$.

According to Ref. [10], for the liquid cannot withstand shear force, the liquid pressure inside the pipe can be expressed directly as the normal displacement of the pipe wall:

$$p_f(a) = \frac{\omega^2 \rho_f J_0(k_{fs}^r a)}{k_{fs}^r J_0'(k_{fs}^r a)} w, \quad (18)$$

where k_{fs}^r is the internal fluid radial wavenumber which can be expressed $(k_{fs}^r)^2 = k_f^2 - k_s^2$, here, $k_f = \omega/c_f$ is the fluid wavenumber and $c_f = \sqrt{B_f/\rho_f}$ is the free-field fluid wavespeed; B_f is the bulk modulus and ρ_f is the density of the internal fluid; J_0 is a Bessel function of order zero; $J_0' = (\partial/\partial \chi)J_0(\chi)$.

It is challenging to give a more realistic coupling equation between soil and pipeline because of the complexity of soil properties. Pipeline and soil are usually defined as two extreme conditions, lubrication contact and compact contact to solve the wavenumber [22]. The actual boundary at pipe-soil interface is not both but a transient state. In recent studies, contact coefficients $\xi \in [0, 1]$ have been used to characterize this uncertain coupling relationship. $\xi = 1$ represents compact contact and $\xi = 0$ represents lubrication contact, then at the pipe soil interface

Lu *et al. Chinese Journal of Mechanical Engineering*   (2022) 35:74

Page 5 of 10

$\xi u = u_x$ $w = u_r$. The force at the interface of the pipe and soil shown by Eq. (14) may be expressed separately by the displacement of the pipe,

$$\begin{cases} \tau_x = T_{11}\xi u + T_{12}w, \\ \tilde{\sigma}_{rr}(a) = T_{21}\xi u + T_{22}w. \end{cases} \tag{19}$$

Substituting Eqs. (18) and (19) into Eq. (17) to eliminate the sine term $\exp(i(\omega t - k_s x))$, The axisymmetric s wave coupled equations of motion can be obtained for the buried fluid-filled pipe, as

$$\begin{cases} [\Omega^2 - (k_s a)^2 + \dfrac{1-v_p^2}{E_p}\dfrac{a^2}{h}T_{11}\xi]U_s - \\ \quad [iv_p(k_s a) - \dfrac{1-v_p^2}{E_p}\dfrac{a^2}{h}T_{12}]W_s = 0, \\ \\ [-iv_p(k_s a) - \dfrac{1-v_p^2}{E_p}\dfrac{a^2}{h}T_{21}\xi]U_s + [1 - \Omega^2 + \delta^2(k_s a)^4 - \\ \quad \dfrac{\rho_f}{\rho_p}\dfrac{a}{h}\dfrac{\Omega^2}{k_{fs}^r a}\dfrac{J_0(k_{fs}^r a)}{J_0'(k_{fs}^r a)} - \dfrac{1-v_p^2}{E_p}\dfrac{a^2}{h}T_{22}]W_s = 0. \end{cases} \tag{20}$$

Solving Eq. (20) can be obtained

$$[\Omega^2 - (k_s a)^2 + \frac{1-v_p^2}{E_p}\frac{a^2}{h}T_{11}\xi]$$
$$[1 - \Omega^2 - \frac{\rho_f}{\rho_p}\frac{a}{h}\frac{\Omega^2}{k_{fs}^r a}\frac{J_0(k_{fs}^r a)}{J_0'(k_{fs}^r a)} - \frac{1-v_p^2}{E_p}\frac{a^2}{h}T_{22}]$$
$$= [iv_p(k_s a) - \frac{1-v_p^2}{E_p}\frac{a^2}{h}T_{12}][iv_p(k_s a) + \frac{1-v_p^2}{E_p}\frac{a^2}{h}T_{21}\xi]. \tag{21}$$

The fluid loading term, FL [11] and the surrounding medium loading matrix, SL, are given by

$$FL = \frac{\rho_f}{\rho_p}\frac{a}{h}\frac{\Omega^2}{k_{fs}^r a}\frac{J_0(k_{fs}^r a)}{J_0'(k_{fs}^r a)}, \tag{22}$$

$$\boldsymbol{SL} = \frac{(1-v_p^2)}{E_p}\frac{a^2}{h}\boldsymbol{T}, \tag{23}$$

then Eq. (21) can be written in a simple form

$$[\Omega^2 - (k_s a)^2 + \xi SL_{11}][1 - \Omega^2 - FL - SL_{22}]$$
$$= [iv_p(k_s a) - SL_{12}][iv_p(k_s a) + \xi SL_{21}]. \tag{24}$$

3 Wave Characteristic

For the $s=1$ wavenumber in buried fluid-filled pipes, $k_1^2 \gg k_L^2$, so $(k_1 a)^2 \gg \Omega^2$. When the frequency is low, $k_{fs}^r \to 0$. According to the properties of Bessel functions,

$\chi \to 0$, $\frac{J_0(\chi)}{J_0'(\chi)} \approx -\frac{2}{\chi}$. Then the fluid loading term, FL, can be simplified as

$$FL = -2\frac{\rho_f}{\rho_p}\frac{a}{h}\frac{\Omega^2}{(k_f^2 - k_s^2)a^2}. \tag{25}$$

Substituting Eq. (25) into Eq. (24) gives

$$k_1^2 = k_f^2(1 + \frac{\beta}{1 - \Omega^2 + \alpha}), \tag{26}$$

where,

$$\begin{cases} \alpha = -SL_{22} - \dfrac{[v_p + iSL_{12}/k_1 a][v_p - i\xi SL_{21}/k_1 a]}{1 - \xi SL_{11}/k_1 a}, \\ \beta = 2\dfrac{a}{h}\left(\dfrac{1-v_p^2}{E_p}\right)B_f, \end{cases} \tag{27}$$

where α stands for the surrounding medium loading and pipe parameters which can be used to evaluate the influence of soil load on the pipe wall displacement. β refers to fluid and pipe parameters which can be used to evaluate the influence of fluid load on the pipe wall displacement. By means of a complex modulus of elasticity Ep (α and β always complex), it is found from Eq. (26) that k_1 is always complex indicating the $s = 1$ wave decays as it propagates. Then α and β are described as the measures of the loading effects of surrounding medium and fluid on the pipe wall respectively. By Eq. (27), β can be obtained directly, but α which is related to the unknown wavenumber k_1 cannot be solved directly. When the pipe is placed in a different medium, the equations can be simplified by boundary conditions.

3.1 Lubrication Contact of Pipe-Medium
On the condition of lubrication contact, the contact coefficient $\xi = 0$, the measure of the loading effects of the surrounding medium $\alpha = -v_p^2 - SL_{22} - iv_p SL_{12}/k_1 a$, then Eq. (24) can be written as

$$k_1^2 = k_f^2(1 + \frac{\beta}{1 - \Omega^2 - v_p^2 - SL_{22} - iv_p SL_{12}/k_1 a}). \tag{28}$$

It can be seen from Eq. (28) that the propagation of k_1 wave will be delayed as it propagates caused by the effect of the pipe wall (i.e., a complex β) and additional damping of the surrounding medium (i.e., a complex α), although there is no frictional damping between pipe and surrounding medium.

3.2 Pipe in Non-Viscous Liquids
For non-viscous liquids, the shear modulus $\mu_m = 0$, contact coefficient $\xi = 0$, as a result, the lame coefficient $\lambda_m = B_m$, the shear wavenumber $k_r \to \infty$, and $\mu_m k_r^2 = \omega^2 \rho_m$. Then

the surrounding medium loading matrix SL can be simplified as $SL_{11} = SL_{12} = 0$. In this case, the measure of the loading effects of the surrounding fluid reduces to $\alpha = -v_p^2 - SL_{22}$. Eq. (24) can be rewritten as

$$k_1^2 = k_f^2(1 + \frac{\beta}{1 - \Omega^2 - v_p^2 - SL_{22}}),\qquad(29)$$

where $SL_{22} = -\frac{\rho_m}{\rho_p} \frac{a^2}{h} \frac{k_L^2}{k_{d1}^r} \frac{H_0(k_{d1}^r a)}{H_0'(k_{d1}^r a)}$. Since SL_{22} is a function of the complex k_1, α is a complex value. So, s_1 wave attenuation is attributed to both material losses along the pipe wall (i.e., a complex β) and radiation losses due to the added damping of the surrounding medium (i.e., a complex α).

3.3 Pie in Air

For an air medium, the loading effects of air on the pipe wall can be neglected, the contact coefficient is considered zero. Then, $T = 0$, $SL = 0$, and $\alpha = -v_p^2$. Eq. (24) can be expressed are consistent with Ref. [13]:

$$k_1^2 = k_f^2(1 + \frac{\beta}{1 - \Omega^2 - v_p^2}).\qquad(30)$$

At low frequency, $\Omega^2 \ll 1$, and $\mathrm{Re}(\beta) \gg 1$, then $k_1^2 > k_f^2$. And that means the wave speed of the $s = 1$ wave will be significantly lower than that of the free wave. In Eq. (30), the imaginary part only exists in β, so the wave attenuation is only due to losses within the pipe wall.

Compared to the equation from Eq. (26) to Eq. (30), it can be seen that, if the real part of α less than zero, $\mathrm{Re}(\alpha) < 0$, external loads of surrounding medium act as additional mass, and the wavenumber will increase compared to the in-air value; Contrarily, if the real part of α more than zero, $\mathrm{Re}(\alpha) > 0$, external loads of surrounding medium act as additional stiffness, and the wavenumber will decrease relative to the in-air case.

4 Numerical Results and Discussions

4.1 Numerical Method

This section presents some numerical results of the shear effect on $s = 1$ wavenumber. The real part k_{re} and imaginary part k_{im} of k_1 are set as variables and the Eq. (24) is described as a target function

Table 1 Properties of the fluid, pipe and surrounding medium

Properties	Fluid	Pipe	Surrounding medium
Density (kg/m³)	1000	2000	2000
Young's modulus (N/m²)	–	5.0×10^9	–
Bulk modulus (N/m²)	2.25×10^9	2013	4.5×10^9
Shear modulus (N/m²)	–	–	$2 \times 10^7 - 10 \times 10^7$
Poisson's ratio	–	0.4	0.481
Material loss factor	–	0.065	–

$$\left\{ \frac{1}{3} \sum_{i=1}^{3} \left[F(k_{re}^{(n)}, k_{im}^{(n)}) - F(\overline{k}_{re}, \overline{k}_{im}) \right]^2 \right\}^{1/2} < \varepsilon,\quad(32)$$

where n is the iterations, $\overline{k}_{re}$, $\overline{k}_{im}$ are the centre of the simplex in the current step, ε is the tolerance. In the calculation process, the derivative of Bessel function can be deal based on its property.
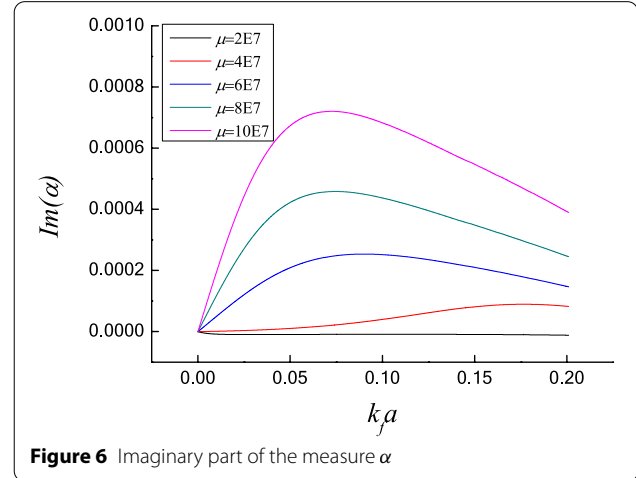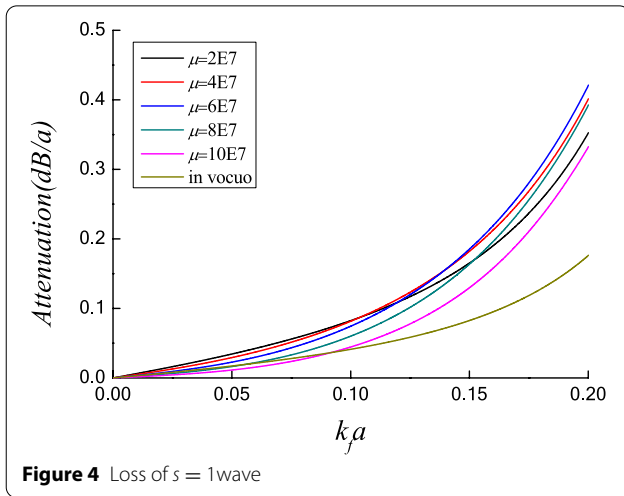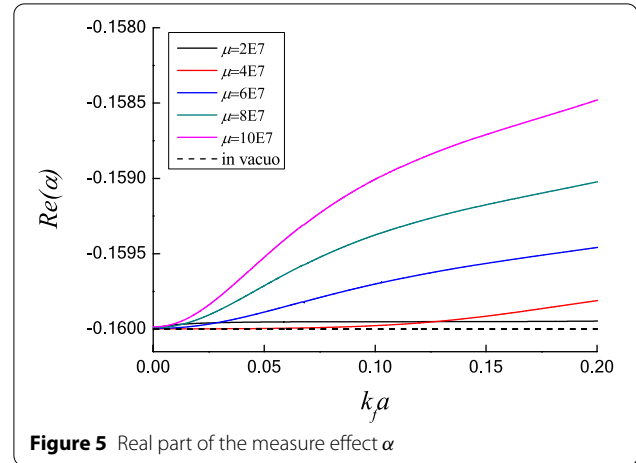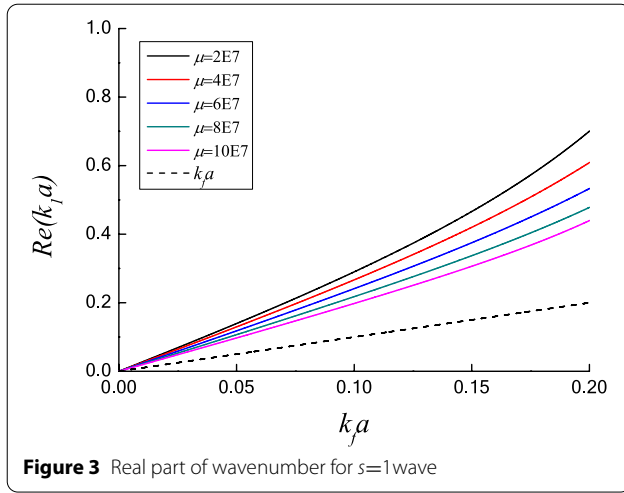
$$\begin{cases} J_0'(k_{fs}^r a) = -J_1(k_{fs}^r a), \\ H_0'(k_{ds}^r a) = -H_1(k_{ds}^r a), \\ H_0''(k_{ds}^r a) = (H_2(k_{ds}^r a) - H_0(k_{ds}^r a))/2, \\ H_1'(k_{rs}^r a) = (-H_2(k_{rs}^r a) + H_0(k_{rs}^r a))/2. \end{cases}\quad(33)$$

For the arguments of the Bessel or Hankel functions are derived from the square root, it is important to choose the sign of the root. The method to choose the sign of the root in Ref. [24] is be used. If the real part is larger, the partial wave can be considered homogeneous and must propagate away from the shell, so the positive square root is chosen. On the other hand, if the imaginary part is larger, the partial wave can be considered inhomogeneous and must decay away from the shell, so the negative square root is selected.

The material properties of the fluid, pipe and surrounding medium are shown in Table 1. Considering the efficiency and convergence, the wavenumbers are calculated up to 1 Hz. The thickness/radius ratio of pipe is 0.125, and the plate compressional wave speed is 1725 m/s.

Considering the previous analysis, the shear effect of surrounding medium and shear effect of pipe-medium interface both affect the wave propagation and attenuation characteristics. This section presents some numeri-

$$F(kr, ki) = \left| \begin{matrix} [\Omega^2 - (k_s a)^2 - SL_{11}][1 - \Omega^2 - FL - SL_{22}] - \\ [iv_p(k_s a) + SL_{12}]^2 \end{matrix} \right| \rightarrow \min.\qquad(31)$$

The Neldes-Mead method [30] is used to solve Eq. (31). In the optimization progress, the termination condition is set as

cal sample to discuss the influence of the shear effects. The attenuations are defined by the loss in dB per unit propagation distance by

Figure 3 Real part of wavenumber for $s=1$ wave

Figure 5 Real part of the measure effect α

Figure 4 Loss of $s = 1$ wave

Figure 6 Imaginary part of the measure α

$$Loss(\text{dB/unit distance } a) = -20\frac{\text{Im}\{k_1 a\}}{\ln(10)}. \qquad (34)$$

4.2 Shear Effect of Surrounding Medium

Some numerical results are shown in this section to explain the influence of the shear effect of surrounding medium. In order to eliminate the effects of surrounding medium and pipe interface friction, the "lubrication contact" assume is used here. Figure 3 gives the wavenumber for the soil with different shear modulus. It can be seen that from Figure 3, as the previous theoretical analysis, the effect of the pipe and surrounding medium is used to substantially increase the real part of the $s = 1$ wavenumber from the free-field value k_f. This solution is similar to Ref. [24]. As the shear effect of the surrounding medium increased, the real part of the wavenumber gradually decreased. The overall loading influences of the surrounding medium are to add mass to the pipe wall, but the shear effect is to add stiffness, and additional stiffness increases with the increase of the shear effect of surrounding medium.

Figure 4 shows the loss in dB per unit propagation distance. Compared with the attenuation in vacuo, the radiation into the surrounding medium is significantly used for much larger attenuation. The attenuation is more serious in the high-frequency range. In fact, at the lower frequency range, the attenuation dominated by losses within the pipe, as the shear effects increased, the attenuation slightly decreased. At higher frequencies, radiation as both compressional waves and shear waves contributes to the attenuation, and then the attenuation increased with the shear effects increased. So the shear effects of surrounding medium should not be neglected in leak detection of buried pipeline.
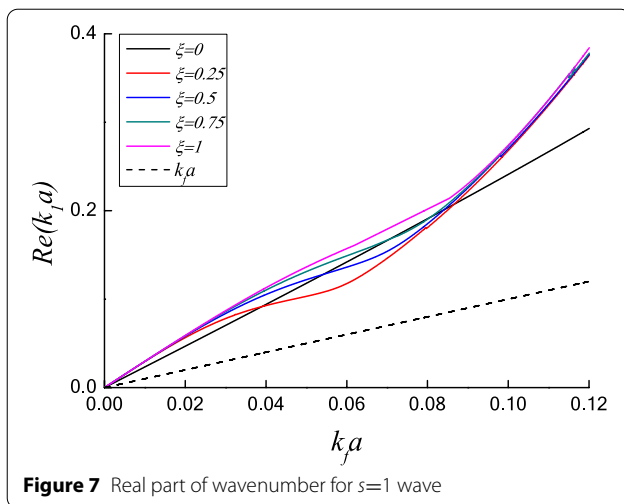
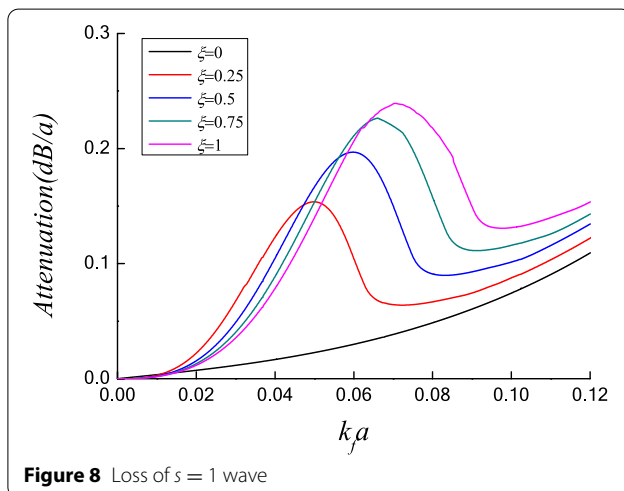**Figure 7** Real part of wavenumber for $s=1$ wave

Figure 8 Loss of $s=1$ wave

In order to better understand the shear effects of surrounding medium on dispersive behaviour of $s=1$ wave, the real and imaginary parts of the measure α are given in Figures 5 and 6 respectively. As shown in these figures, the level of $\text{Re}(\alpha)$ is much larger than $\text{Im}(\alpha)$, thus $\text{Re}(\alpha)$ plays a dominant role in the overall loading effects of surrounding medium on the propagation characteristics. As mentioned above, a negative $\text{Re}(\alpha)$ indicates that the surrounding medium is to add mass to the pipe wall and the propagation wavenumber will be increased. With the increase of the shear effects, $\text{Re}(\alpha)$ increased and slightly larger than the value in vacuo, thus the shear effects of surrounding medium have some impact on the propagation characteristics of $s=1$ wave. Additionally, it can be noted that $\text{Re}(\beta)$ ($\text{Re}(\beta)=0.58$) is much larger than $\text{Re}(\alpha)$, which shows the fluid loading dominants the vibration of

the pipe wall for plastic pipe, so more attention should be paid to fluid load wave in leak detection.

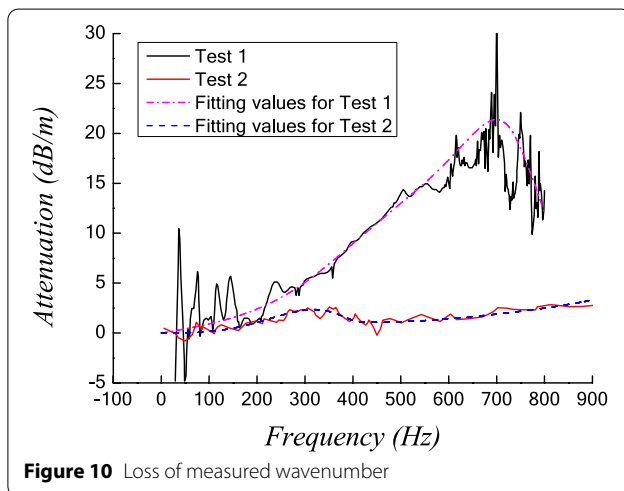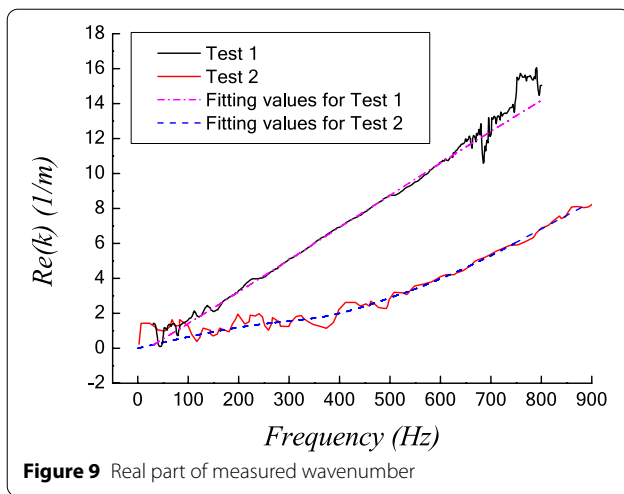### 4.3 Shear Effects at the Pipe/Medium Interface

The shear effects at the pipe/medium interface exist in buried pipe systems, but it is normally ignored because the coupling relationship between pipes and surrounding medium is not clear. Figure 7 and Figure 8 show the wavenumber for $s=1$ wave with different contact coefficients. In calculation, the shear wave speed of surrounding medium is set to 300 m/s.

As shown in Figure 7, the real part of wavenumber for $s=1$ wave much larger than the free-field value k_f with different contact coefficients. Whether the shear effect of the interface between surrounding medium and pipe wall has a great influence on the real part at high frequency ($k_f a > 0.09$). Once these shear effects are included, the influence of the contact coefficient on the real part is mainly reflected in the middle frequency band ($k_f a \in (0.02, 0.09)$). In Figure 8, it can be seen that with the consideration of the shear effect of the interface, more waves can be radiated into the surrounding medium. The attenuation increased as the frequency increased, and has a local peak in the middle frequency band. The frequency corresponding to these peaks increased with the contact coefficient increased. The local peak of attenuation is caused by the resonance between the additional mass of the surrounding medium and the pipe wall, resulting in a dramatic increase in the wave intensity of radiation to the surrounding medium. At the high frequency, the friction force between surrounding medium and pipe wall seems not enough for surrounding medium to vibrate with the pipe wall, so the results of attenuation gradually approaching the value in the case of lubrication contact.

In engineering applications, the actual wave number and attenuation should be obtained according to the actual pipe-soil coupling situation, and the delay estimation should be carried out according to the leakage signal dispersion in order to obtain the accurate leakage location results. Medium and low-frequency signal is generally be used, and the contact coefficient which has a certain influence on the propagation characteristics of the wave in this frequency band should not be ignored.

4.4 Field Test

This section presents some numerical results of wavenumber from actual plastics water pipes. Two field tests were carried out for pipes in different buried environments. The details of the experimental setup and analysis for test 1 can be found in Refs. [21, 24]. The test 2 selected the water supply network in Southwest Jiaotong

Lu *et al. Chinese Journal of Mechanical Engineering*   (2022) 35:74

Page 9 of 10

Figure 9 Real part of measured wavenumber

Figure 10 Loss of measured wavenumber

effects at the pipe/medium interface, the attenuations have a local peak (about 700 Hz in test 1 and 320 Hz in test 2), which consistent with the present predictions.

5 Conclusions

(1) Axisymmetric waves in thin-walled fluid-filled plastic pipe surrounded by an infinite elastic medium which can sustain both longitudinal and shear waves have been studied. The contact coefficient has been introduced to describe the contact strength of pipe and surrounding medium. Then a general expression for the fluid-dominated wavenumber has been presented in buried fluid-filled plastic pipe.

(2) For axisymmetric waves, the fluid loading dominates the vibration of the plastic pipe wall. The overall loading effects of the surrounding medium are to add mass to the pipe wall, but the shear effect is to add stiffness, which increases with the shear effect of surrounding medium. The shear effect of the surrounding medium also influences the attenuation of the wave.

(3) The added mass of the surrounding medium will resonate with the pipe wall at a specific frequency under the shear effects at the pipe/medium interface, resulting in the change of the propagation characteristics of the wave near the frequency. At higher frequency, the influence of shear effects at the interface on the propagation characteristics is not obvious. The wavenumber can be solved by compact contact theory and the attenuation will approximate the lubricating contact state with the frequency increases.

University, the sensor is set in the pipe well, and fire hydrant discharge signal as leakage signal. The distance from pipe well to hydrant discharge is 12 m. The soil and pipe coupling parameters cannot be obtained in both tests, the theoretical calculation and experimental comparison are not presented in this paper.

Figures 9 and 10 show the real and the imaginary components of the measured and fitting wavenumbers. Due to the different buried environments of pipes in the two tests, both the real and imaginary components of the measured wavenumbers are large different. There are some reflections from pipe connections blow 160 Hz which cause some fluctuations at the corresponding frequency. At the high frequency the measured data becomes unreliable due to the noise interference. Experimental measurements show good agreement on the trend of the wavenumbers with predictions in Figures 7 and 8. Due to the shear

Authors' Information
Ping Lu, born in 1982, is currently a PhD candidate at *State Key Laboratory of Traction Power, Southwest Jiaotong University, China*. He received his master degree on Bridge and Tunnel Engineering from *Chongqing University, China*, in 2008. His research interests include sound and vibration.
Xiaozhen Sheng, born in 1962, is currently a professor at *School of Urban Railway Transportation, Shanghai University of Engineering Science, China*. He received his doctor degree on sound and vibration from *Southampton University, UK*, in 2001.
Yan Gao, born in 1976, is currently a professor at *Key Laboratory of Noise and Vibration Research, Institute of Acoustics, Chinese Academy of Sciences, China*. She received her doctor degree on sound and vibration in *Southampton University, UK*, in 2006.

Lu *et al. Chinese Journal of Mechanical Engineering*   (2022) 35:74

Page 10 of 10

Ruichen Wang, born in 1989, is currently a researcher at *Institute of Railway Research, University of Huddersfield, UK*. He received his doctor degree on vehicle engineering from *University of Huddersfield, UK*, in 2016.

Author Details
[1]State Key Laboratory of Traction Power, Southwest Jiaotong University, Chengdu 610031, China. [2]School of Urban Railway Transportation, Shanghai University of Engineering Science, Shanghai 201620, China. [3]Key Laboratory of Noise and Vibration Research, Institute of Acoustics, Chinese Academy of Sciences, Beijing 100190, China. [4]Institute of Railway Research, University of Huddersfield, Huddersfield HD1 3DH, UK.

References
[1] H Fuchs, R Riehle. Ten years of experience with leak detection by acoustic signal analysis. *Applied Acoustics*, 1991, 33: 1–19.
[2] J M Muggleton, M J Brennan, P W Linford. Wavenumber prediction of waves in buried pipes for water leak detection. *Journal of Sound and Vibration*, 2002, 249: 939–954.
[3] O Hunaidi, A Wang. A new system for locating leaks in urban water distribution pipes. *Management of Environmental Quality*, 2006, 7(4): 450–466.
[4] Y Gao, M J Brennan, P F Joseph. A comparison of time delay estimators for the detection of leak noise signals in plastic water distribution pipes. *Journal of Sound and Vibration*, 2006, 292: 552–570.
[5] J Wang, L Zhao, T Liu, et al. Novel negative pressure wave-based pipeline leak detection system using fiber bragg grating-based pressure sensors. *Journal of Lightwave Technology*, 2017, 35(16): 3366–3373.
[6] J Hong, W Song. Delta-modulated cross-correlation method for delay estimation on source localization. Asia-pacific Signal and Information Processing Association Annual Summit and Conference, 2017: 1516–1519.
[7] K S Ng, P Y Chen, Y C Tseng. A design of automatic water leak detection device. Proceedings of the IEEE Conference on Opto-electronic Information Processing, Singapore July 7-9, 2017: 70–73.
[8] Y Ma, Y Gao, X Cui, et al. Adaptive phase transform method for pipeline leakage detection. *Sensors*, 2019, 19: 310.
[9] M J Brennan, Y Gao, P F Joseph. On the relationship between time and frequency domain methods in time delay estimation for leak detection in water distribution pipes. *Journal of Sound and Vibration*, 2007, 304: 213–223.
[10] C R Fuller, F J Fahy. Characteristics of wave-propagation and energy distributions in cylindrical elastic shells filled with fluid. *Journal of Sound and Vibration*, 1982, 81: 501–518.
[11] C R Fuller. The input mobility of an infinite circular cylindrical elastic shell filled with fluid. *Journal of Sound and Vibration*, 1983, 87: 409–427.
[12] M Xu, W Zhang. Vibrational power flow input and transmission in a circular cylindrical shell filled with fluid. *Journal of Sound and Vibration*, 2000, 234: 387–403.
[13] R J Pinnington, A R Briscoe. Externally applied sensor for axisymmetric waves in fluid-filled pipe. *Journal of Sound and Vibration*, 1994, 173(4): 503–516.
[14] R J Pinnington. The axisymmetric wave transmission properties of pressurized flexible tubes. *Journal of Sound and Vibration*, 1997, 204: 271–289.
[15] R J Pinnington. Axisymmetric wave transfer functions of flexible tubes. *Journal of Sound and Vibration*, 1997, 204: 291–310.
[16] B K Sinha, T J Plona, S Kostek, et al. Axisymmetric wave propagation in fluidloaded cylindrical shells. I: theory. *Journal of the Acoustical Society of America*, 1992: 1132.
[17] J E Greenspon. Vibrations of thick and thin cylindrical shells surrounded by water. *Journal of the Acoustical Society of America* 1961, 33: 1321.
[18] R Long, P Cawley, M J S Lowe. Acoustic wave propagation in buried iron water pipes. *Proc Royal Soc Lond: Mathematical, Physical and Engineering Sciences*, 2003, 459: 2749–2770.
[19] J Zhang, L Jia, Y Shu, Wave propagation characteristics of the shells of revolution by frequency wave number spectrum method. *Journal of Sound and Vibration*, 2002, 251(2): 367–372.
[20] J M Muggleton, M J Brennan, R J Pinnington. Wavenumber prediction of waves in buried pipes for water leak detection. *Journal of Sound and Vibration*, 2002, 249: 939–54.
[21] J M Muggleton, M J Brennan, P W Linford. Axisymmetric wave propagation in fluid-filled pipes: Wavenumber measurements in vacuo and buried pipes. *Journal of Sound and Vibration*, 2004, 270: 171–190.
[22] J M Muggleton, J Yan. Wavenumber prediction and measurement of axisymmetric waves in buried fluid-filled pipes: Inclusion of shear coupling at a lubricated pipe/soil interface. *Journal of Sound and Vibration*, 2013, 332: 1216–1230.
[23] Y Gao, F Sui, J M Muggleton, et al. Simplified dispersion relationships for fluid-dominated axisymmetric wave motion in buried fluid-filled pipes. *Journal of Sound and Vibration*, 2016, 375: 386–402.
[24] Y Gao, Y Liu, J M Muggleton. Axisymmetric fluid-dominated wave in fluid-filled plastic pipes: Loading effects of surrounding elastic medium. *Applied Acoustics*, 2017, 116: 43–49.
[25] M K Kalkowski, J M Muggleton, E Rustighi. Axisymetric semi-analytical finite elements for modeling waves in buried/submerged fluid-filled waveguides. *Computer and Structures*, 2018, 196: 327–340.
[26] S Yan, H Yang, Y Gao, et al. On image fusion of ground surface vibration for mapping and locating underground pipeline leakage: An experimental investigation. *Sensors*, 2020: 1–20.
[27] A W Leissa. *Vibration of Shells*, NASA SSP-288, Washington DC: US Government Printing Office, 1973.
[28] W M Ewing, W S Jardetzky, F Press. *Elastic waves in layered media*. New York: McGraw-Hill, 1957.
[29] M C Junger, D Feit Sound. *Structures and Their Interaction*. Cambridge: Cambridge Press, 1972.
[30] B Xue, D Cui, L Li, et al. Parallel inverse design method of wheel profile. *Journal of Mechanical Engineering*, 2013, 49(16): 8–16. (in Chinese)